Structural and thermodynamic characterization of a cytoplasmic dynein light chain–intermediate chain complex

John C. Williams*[†‡], Petra L. Roulhac[§], Anindya G. Roy[¶], Richard B. Vallee[¶], Michael C. Fitzgerald[§], and Wayne A. Hendrickson[‡‖]**

*Department of Biochemistry and Molecular Biology and [†]Kimmel Cancer Center, Thomas Jefferson University, Philadelphia, PA 19107; Departments of [‡]Biochemistry and Molecular Biophysics and [¶]Pathology and Cell Biology, and [‖]Howard Hughes Medical Institute, Columbia University, New York, NY 10032; and [§]Department of Chemistry, Duke University, Durham, NC 27708

Contributed by Wayne A. Hendrickson, April 23, 2007 (sent for review December 21, 2006)

Cytoplasmic dynein is a microtubule-based motor protein complex that plays important roles in a wide range of fundamental cellular processes, including vesicular transport, mitosis, and cell migration. A single major form of cytoplasmic dynein associates with membranous organelles, mitotic kinetochores, the mitotic and migratory cell cortex, centrosomes, and mRNA complexes. The ability of cytoplasmic dynein to recognize such diverse forms of cargo is thought to be associated with its several accessory subunits, which reside at the base of the molecule. The dynein light chains (LCs) LC8 and TcTex1 form a subcomplex with dynein intermediate chains, and they also interact with numerous protein and ribonucleoprotein partners. This observation has led to the hypothesis that these subunits serve to tether cargo to the dynein motor. Here, we present the structure and a thermodynamic analysis of a complex of LC8 and TcTex1 associated with their intermediate chain scaffold. The intermediate chains effectively block the major putative cargo binding sites within the light chains. These data suggest that, in the dynein complex, the LCs do not bind cargo, in apparent disagreement with a role for LCs in dynein cargo binding interactions.

crystal structure | microtubules | molecular transport | protein–protein interaction

The dynein motor is a large multisubunit protein that binds to microtubules and hydrolyzes ATP to generate force toward the minus end of microtubules. Cytoplasmic dynein 1 is responsible for almost all cytoplasmic activities. It is a large (1.2 MDa) complex composed of four principal homodimeric components: the dynein heavy chain (HC) (≈530 kDa) (1), intermediate chain (IC) (74 kDa), light intermediate chain (LIC) (two members, 30 and 50 kDa), and light chains (LCs) (three members, 10, 12, and 14 kDa) (2). The C-terminal region of the dynein HC represents the motor domain and contains six AAA elements, the first and third of which hydrolyze ATP (3). Hydrolysis of ATP by these domains indirectly acts on the microtubule binding region that lies between the fourth and fifth AAA repeats to generate force (4).

The N-terminal region of the dynein HC constitutes the base, or tail, of the molecule and contains the self-association, IC, and LIC binding sites (5). The ICs also contain binding sites for the LCs (2). Members of each subunit class have been implicated in cargo binding. The ICs bind to kinetochores and to the Golgi apparatus through an interaction with the $p150^{Glued}$ subunit of another complex, dynactin (6). Additional potential direct IC–cargo interactions have also been reported (7). An interaction between the LICs and pericentrin, a centrosomal form of cargo, has also been identified (8).

Three classes of LC have been identified, TcTex1 (DYNLT1/3), LC8 (DYNLL1/2), and LC7 (DYNLRB1/2) (9). Each binds to the ICs at discrete sites separate from the dynactin $p150^{Glued}$ binding site and before the WD-repeat domain that binds the HC. Whereas the number of direct interactions involving the LICs and ICs is limited, the LCs have been found in interaction screens involving a large number of binding partners, including BimL (10), nNOS (11), TRPS1 (12), NRF-1 (13), Pak1 (14), rhodopsin (15), BMPRII (16), Fyn (17) and SATB1 (18). Despite the large number of targets and apparent promiscuity, there is no overlap in the targets between the different classes of LCs. Together, these data have suggested that the LCs provide the molecular complexity and binding specificity to play a substantial role in linking cytoplasmic dynein to a wide range of cargo forms.

Very little high-resolution structural information is available for the dynein complex, despite its importance in a broad range of biological functions and diseases. To gain insight into the structural relationship between the LCs and ICs, we have obtained structural and thermodynamic data of TcTex1 and LC8 bound to a 32-residue fragment of the intermediate chain. We report that the ICs sequester the LCs in a manner that precludes coordinate interactions between dynein and many proposed cargo proteins.

Results

Crystallization and Diffraction Analysis. LC8 and TcTex1 were crystallized with a 32-residue fragment of the IC (residues 104–138 based on human IC2C, GenBank entry AF134477). The diffraction images indicated considerable diffuse scattering, and the crystals were sensitive to radiation, limiting diffraction to Bragg spacings of 2.8 Å. Crystals were generated from selenomethionyl (SeMet) TcTex1, and diffraction data were collected at the anomalous peak of selenium (Table 1). This crystal is in space group $C222_1$ with a unit cell of $a = 116.97$ Å, $b = 119.87$ Å, and $c = 211.70$ Å. The selenium positions were obtained from an initial molecular-replacement model based on the TxTex1 structure, and the anomalous signal was used to generate experimental phase information (19). The initial maps were readily interpretable and indicated that there are two complexes per asymmetric unit (Table 2).

Author contributions: J.C.W., R.B.V., M.C.F., and W.A.H. designed research; J.C.W. and P.L.R. performed research; A.G.R. and R.B.V. contributed new reagents/analytic tools; J.C.W., P.L.R., M.C.F., and W.A.H. analyzed data; and J.C.W., P.L.R., R.B.V., M.C.F., and W.A.H. wrote the paper.

The authors declare no conflict of interest.

Freely available online through the PNAS open access option.

Abbreviations: HC, heavy chain; IC, intermediate chain; LIC, light intermediate chain; LC light chain.

Data deposition: The atomic coordinates and structure factors have been deposited in the Protein Data Bank, www.pdb.org (PDB ID code 2PG1).

**To whom correspondence should be addressed. E-mail: wayne@convex.hhmi.columbia.edu.

This article contains supporting information online at www.pnas.org/cgi/content/full/0703614104/DC1.

Table 1. Diffraction data

Wavelength, Å	0.9791
Bragg spacings, Å	20–2.8
Reflections	
Measured	411,870
Unique	36,881
Completeness, %	99.9 (100.0)
$I/\sigma(I)$	31.3 (6.8)
R_{sym}	8.5 (36.2)

Values in parentheses are for the last shell.

Table 2. Refinement statistics

Bragg spacings, Å	20–2.8
R/R_{free}	20.8%/25.3%
Reflections, R/R_{free}	36,416/1,815
Completeness, %	98.5 (90.0)
Atoms, protein/waters	6,928/24
Stereochemical ideality (rmsd)	
Bonds, Å/angles, °	0.008/1.4
B-factor rmsds, Å^2	
MC bonds/angles	1.76/2.47
SC bond/angles	3.09/4.65
Mean B-factors (Å^2)	
MC/SC/water	24.9/27.5/50.9
Ramachandran analysis	
Favored/allowed, %	92.2/98.9

MC, main chain; SC, side chain; rmsd, root-mean-squared deviation.

Overall Structure. The structure shows that LC8, TcTex1, and the IC fragments form a 2:2:2 stoichiometric complex in which IC fragments lie in clefts on the outside of LC dimers, much like railroad tracks (Fig. 1 *A* and *B*). The IC peptides are oriented in the same N to C terminus direction. Each LC has a twofold axis, and the IC fragments run roughly parallel to each LC axis. Residues 112–124 of the IC interact with TcTex1, and residues 131–138 interact with LC8. There is a significant bend in the IC between the TcTex1 and LC8 binding sites that is reflected in dramatically different Ramachandran angles for these residues. The residues that comprise this region, Arg_{125}-Glu-Ile-Val_{128}, are completely conserved in mammals and highly conserved in lower eukaryotes. It is also worth noting that the side chains of the conserved Ile and Val are completely solvent-exposed, although the functional relevance of this is not clear. There is no break in the electron density for these residues (Fig. 1*C*).

The average buried surface areas for the individual IC–LC8 and IC–TcTex1 interfaces are 1,378 ± 78 Å^2 and 1,932 ± 76 Å^2, respectively (20). The average buried surface area for the full complex is very large, 6,661 Å^2. The contact between LC8 and TcTex1 within each complex is minimal (<100 Å^2) and through nonconserved residues.

TcTex1–IC Interface. This complex also represents the first structure of TcTex1 with a natural ligand. Although TcTex1 and LC8 bind distinct (nonoverlapping) targets, the ligand binding properties of TcTex1 and LC8 are remarkably similar. Moreover, the LC8–IC interaction is very similar to that of LC8–nNOS (21). The extended IC peptide binds to the domain-swapped β-strand of the dimeric TcTex1 and places hydrophobic residues at positions in TcTex1 equivalent to the hydrophobic pockets of LC8 [Fig. 2*A* and supporting information (SI) Fig. 5]. Thus, the same "geometric specificity" used by LC8 to bind to a large number of targets also applies to TcTex1. Several notable differences between TcTex1 and LC8 do affect target specificity, however. First, the β-strands of TcTex1 are longer than those in LC8 (Fig. 2*B*); thus, the interface between the IC peptide and TcTex1 is extended to include three additional backbone hydrogen bonds. Second, the α2-helix in TcTex1 is splayed away from the β-sheet, as in apo-TcTex1 (22); whereby helix capping by a glutamine residue conserved in all LC8 targets (Fig. 2*C*, red circle) cannot occur (22, 23). Instead, the equivalent residue in IC (Fig. 2*A*, red shading) hydrogen bonds to conserved TcTex1 side chains (SI Fig. 5). Third, there are several additional hydrophobic interactions with TcTex1 at the N-terminal region of the IC interface (Fig. 2*A*), including a pocket that binds the completely conserved Leu-112 in the IC. Previous studies showed that L112A mutation abolished the IC–TcTex1 interaction (24) (A. Dawn and J.C.W., unpublished data).

The IC peptide fragment used in for the crystallization contains the residues RRXXR at its N terminus (where X is any residue), which has been suggested as a TcTex1 recognition sequence (24). This segment is disordered in the structure, and thus it does not constitute a TcTex1 binding motif as has been previously reported.

Thermodynamic Analysis of IC–LC Complex. The structure shows that both binding pockets in each LC dimer are occupied in the

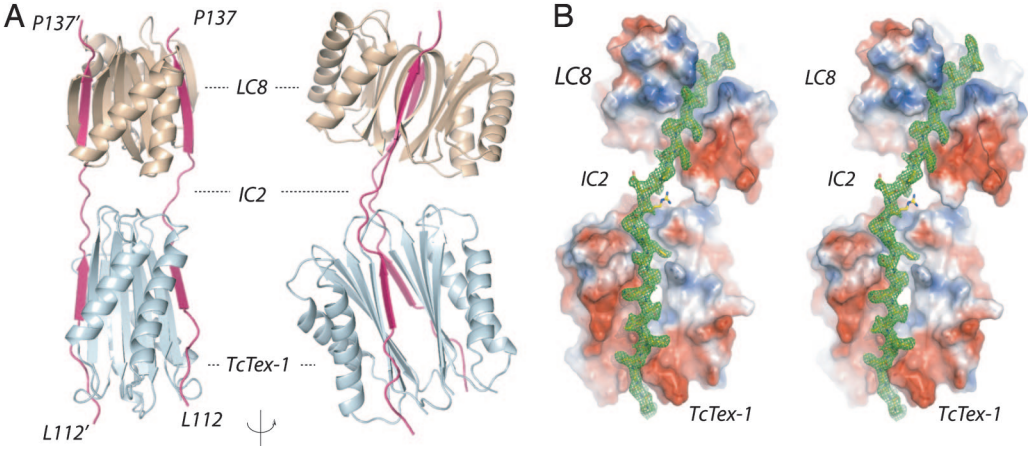

Fig. 1. Ribbon diagram of the dynein complex. (*A*) TcTex1 (cyan) and LC8 (wheat) homodimers are associated with two IC peptides (residues 104–138; magenta). Each IC peptide binds to one side of each LC dimer producing a 2:2:2 complex. Residues 112–124 of the IC contact TcTex1, and residues 129–137 contact LC8. Two views are shown, rotated by 90° about the vertical axis. (*B*) Experimental electron density of the IC peptide in green on the electrostatic surface of LC8 and TcTex1 (54) in stereo.

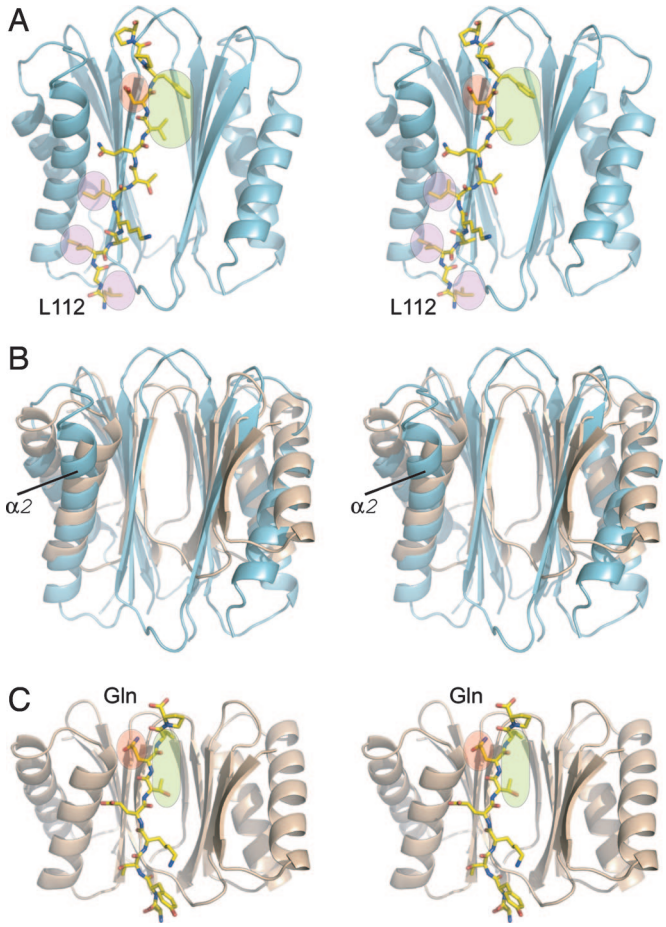

Fig. 2. Common features of the LC-target interactions. (*A*) Stereoview of TxTex1 (cyan ribbon) and the IC peptide (stick representation). The IC residue, D121, highlight by the red oval is equivalent to the invariant glutamine found in all LC8 target peptides. The green area indicates the hydrophobic contacts between the IC and TcTex1. This region also maps to an equivalent site in LC8. The pink highlighted regions indicate additional hydrophobic sites that may contribute to target specificity. Mutation of L112 to alanine abrogated the TcTex1–IC interaction (24) (A. Dawn and J.C.W., unpublished data). (*B*) Superposition of β-strands of TcTex1 (cyan) and LC8 (wheat). Although TcTex1 and LC8 are structurally similar, TcTex1 is generally extended compared with LC8. This extension results in additional contacts for the IC peptide. Also note that the α2-helix bends away from the IC peptide. (*C*) Stereoview of LC8 (wheat ribbon) and the IC peptide (stick representation). The invariant glutamine is highlighted in red. The hydrophobic binding pockets are highlighted in green.

complex with ICs, which suggests that there should be enhancement of binding affinity due to multivalency (25) (see *Discussion*). Our initial attempts to measure such affinity enhancement were complicated by the weak dimerization of the LCs (26) and weak intrinsic affinity of the peptide targets. Thus, we turned to an alternative method, SUPREX (27–30), to analyze the thermodynamic stability of the complex in the absence and presence of a series of different peptide and protein ligands (see Table 3).

This method follows the hydrogen/deuterium exchange of the amide backbone for one or more species at increasing concentrations of denaturant in deuterated buffers using mass spectrometry. A decrease in free energy resulting from an interaction shifts the denaturation point of bound protein to higher denaturant concentrations.

For these studies, we used the monomeric IC peptide that was used in our crystallographic studies (denoted here on as IC_{MONO}), an IC fragment that includes the LC binding sites and a dimerization domain C-terminal from the LC8 binding site

Table 3. Summary of SUPREX-derived thermodynamic parameters for LC8 and its complexes

	ΔG_f, kcal/mol	m,* kcal/mol	$\Delta\Delta G_f$,*† kcal/mol
LC8[1]‡	−12.3 ± 0.1	1.3 ± 0.1	0
LC8[2a] + IC_{MONO}[2b]	−12.6 ± 0.1	1.4 ± 0.2	−0.3 ± 0.1
LC8[2a] + nNOS[2b]	−13.2 ± 0.1	1.4 ± 0.1	−0.9 ± 0.1
LC8[3a] + IC_{MONO}[3b] + TcTex1[3c]	−13.7 ± 0.1	1.3 ± 0.2	−1.4 ± 0.1
LC8[1] + TcTex1[1]	−12.3 ± 0.2	1.4 ± 0.1	−0.0 ± 0.2

*Errors are the standard error of fitting.
†Value relative to LC8 alone.
‡Protein concentration is based on dimer: 1, 85 μM; 2a, 77 μM; 2b, 442 μM; 3a, 65 μM; 3b, 374 μM; 3c, 130 μM.

(residues 104–249, hereafter denoted IC_{DIMER}) (31) (J. M. Donaldson, J. D. Lear, and J.C.W., unpublished data) and a nNOS peptide (21) in tests with LC8 and TcTex1. Interactions were monitored by SUPREX analyses on LC8 and included the acquisition of a series of different SUPREX curves (mass vs. denaturant concentration) using H/D exchange times that varied between 30 and 150 min (SI Table 4) as well as studies in the presence of the various ligands in this study using an H/D exchange time of 45 min (Fig. 3 *A* and *C*).

To obtain the free energy of binding, the $C_{SUPREX}^{1/2}$ values obtained at the different H/D exchange times (SI Table 4) were used to generate plots of ΔG_{app} versus the observed $C_{SUPREX}^{1/2}$ value (Eq. **1**). The plots generated for apo-LC8 and LC8 in the presence of IC_{MONO}, nNOS, and both IC_{MONO} and TcTex1 are shown in Fig. 3*B*. The lines in each plot represent the best fit of the data to a line using a linear least squares analysis. According to Eq. **1**, the slope and y intercept of each line correspond to the m value and ΔG_f (respectively) of LC8 and each LC8 complex. The m and ΔG_f values obtained from the data in Fig. 3*B* are summarized in Table 3. Correlation coefficients greater than 0.98 were obtained in the linear least-squares analyses performed on each data set.

$$\Delta G_{app} = \Delta G_f + m C_{SUPREX}^{1/2}, \quad [1]$$

where

$$-\Delta G_{app} = RT \ln\left(\frac{\left(\frac{\langle k_{int}\rangle t}{0.693} - 1\right)}{\frac{n^n}{2^{n-1}}(P^{n-1})}\right).$$

The accurate measurement of SUPREX-derived m and ΔG_f values for LC8 using Eq. **1** requires that the protein folding/unfolding reaction of LC8 is reversible and well modeled by a two-state process in which partially folded intermediate states are not involved. The chemical denaturation of LC8 induced by guanidinium chloride (GdmCl) has been shown to be reversible, but it involves at least three states including folded dimer, folded monomer, and unfolded monomer (26). Because of this non-two-state folding behavior of LC8, our SUPREX-derived m and ΔG_f values do not accurately describe the biophysical properties of the LC8 unfolding/refolding reaction. However, we have previously shown that when SUPREX data obtained on non-two-state folding proteins are well fit to Eq. **1** (as is the case with our LC8 data), the resulting ΔG_f values extracted for a given protein system can be used to generate accurate $\Delta\Delta G_f$ values (27). Thus, whereas the SUPREX-derived ΔG_f values in Table 3 are not expected to be accurate, the $\Delta\Delta G_f$ values in the table are expected to be reasonably accurate.

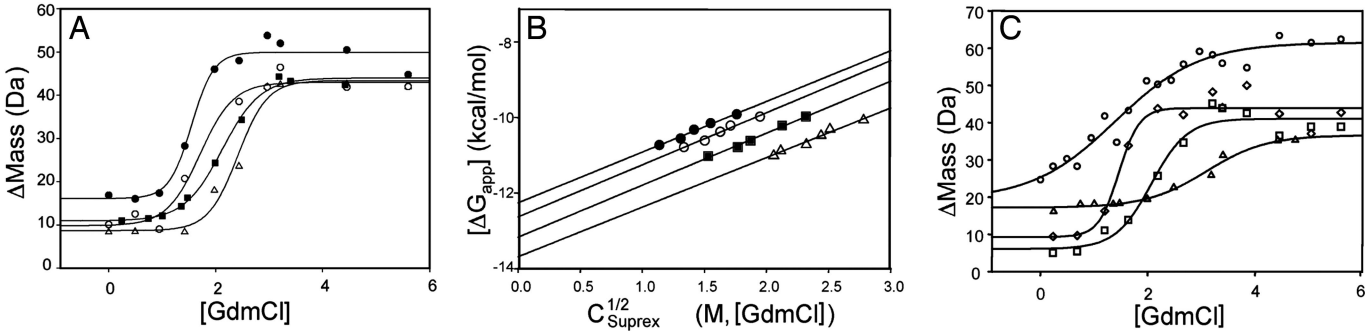

Fig. 3. Thermodynamic analysis. (*A*) SUPREX curves for 85 μM LC8 (filled circles), 77 μM LC8 in the presence of 442 μM IC_{MONO} (open circles), 77 μM LC8 in the presence of 442 μM nNOS peptide (filled squares), and 130 μM LC8 in the presence of 374 μM IC_{MONO} and 130 μM TcTex1 (open triangles). All curves shown were subjected to an H/D exchange time of 45 min. (*B*) The $-RT\ln[((\langle k_{int}\rangle t/0.693) - 1)/((n^n/2^{n-1})[P]^{n-1})]$ (i.e., $-\Delta G_{app}$) versus $C^{1/2}_{SUPREX}$ plots obtained for LC8 (filled circles), LC8 in the presence of IC_{MONO} (open circles), LC8 in the presence of nNOS peptide (filled squares), and LC8 in the presence of IC_{MONO} and TcTex11 (open triangles). Protein and peptide concentrations are the same as in *A*. (*C*) SUPREX curves for 10 μM LC8 (open circles), 9 μM LC8 in the presence of 454 μM IC_{MONO} (open diamonds), 8 μM LC8 in the presence of 417 μM IC_{MONO} and 8 μM TcTex1 (open squares), and 13 μM LC8 in the presence of 35 μM IC_{DIMER} (open triangles). All curves shown were subjected to an H/D exchange time of 45 min.

The SUPREX-derived $\Delta\Delta G_f$ values in Table 3 reveal that binding of the nNOS peptide to LC8 is tighter than the binding of the IC_{MONO} to LC8 alone. It is also clear that the binding of the IC_{MONO} to LC8 is significantly enhanced in the presence of TcTex1. This increased binding affinity confirms multivalency effects, because TcTex1 has no measurable effect on the ΔG_f of LC8 in an equimolar mixture of LC8 and TcTex1 (see Table 3). We note that the $\Delta\Delta G_f$ value determined for the LC8–IC peptide complex is barely measurable in our experiments given the precision of our measurements. However, the $\Delta\Delta G_f$ values associated with the LC8–nNOS and LC8–IC_{MONO}–TcTex1 complexes are significant; and it is clear that an avidity effect of $\approx$1 kcal/mol was measured for the binding of the IC_{MONO} peptide to LC8 in the presence of TcTex1. The 1 kcal/mol effect measured in our experiment establishes a lower limit of the total effect. Unfortunately, establishing the true binding affinity (e.g., K_D value) for the IC_{MONO} to LC8 when this ligand is preorganized on TcTex1 is complicated in our experiments because such a calculation requires that the concentration of free IC_{MONO}–TcTex1 complex in our solution be known. This cannot be determined without a known IC_{MONO}–TcTex1 binding constant. Nonetheless, our SUPREX results serve to establish that there is an avidity effect with TcTex1 and that this effect results in at least an order of magnitude increase in the binding free energy of the IC_{MONO} peptide to LC8. Such a conclusion can be drawn in the absence of a known IC_{MONO}–TcTex1 binding constant because the concentration of LC8 relative to the IC_{MONO} in our experiments with and without the TcTex1 peptide was relatively constant.

Although the data indicate that the presence of TcTex1 significantly increases the binding energy of the IC_{MONO} peptide to LC8 through multivalent interactions, each IC_{MONO} peptide contains only a single LC8 binding sequence (and a single TcTex1 binding). Consequently, it is not a bivalent ligand, and the substantial gain in free energy to be expected from a bivalent ligand interacting with a bivalent receptor is not realized. Thus, we turned to a larger fragment of the IC that was recently demonstrated to be dimeric (31) (J. M. Donaldson, J. D. Lear, and J.C.W., unpublished data) to mimic the natural bivalent IC ligand for LC8.

The SUPREX curve obtained for the LC8–IC_{DIMER} complex is shown in Fig. 3*C*. Limited solubility of IC_{DIMER} prevented the full analysis carried out for the peptides described above. Nonetheless, SUPREX curves obtained on LC8 at similar concentrations (i.e., $\approx$5 μM) and in the presence of IC_{MONO} and TcTex1 were collected for direct comparison (Fig. 3*C*). The $C^{1/2}_{SUPREX}$ values obtained at these low protein concentrations for LC8 alone, the LC8–IC_{MONO} complex, the LC8–IC_{MONO}–TcTex1 complex, and the LC8–IC_{DIMER} complex were 1.4, 1.5, 2.1, and 3.1 M GdmHCl, respectively. The $C^{1/2}_{SUPREX}$ value for the LC8–IC_{DIMER} complex was shifted to the highest denaturant concentration, suggesting that IC_{DIMER} was bound tighter to LC8 than either the IC_{MONO} peptide or the IC_{MONO} peptide in the presence of TcTex1. Our SUPREX analyses of LC8 at the 5 μM concentration did not permit an evaluation of ΔG_f or m values, because the $C^{1/2}_{SUPREX}$ values obtained form SUPREX curves recorded at different H/D exchange times were not well fit to Eq. **1**. Presumably, the potential population of a monomeric state at these concentrations complicated quantitative analyses. Thus, our analysis of the IC_{DIMER} binding to LC8 is strictly qualitative, and our conclusion that IC_{DIMER} is the tightest-binding ligand to LC8 is based solely on the relative position of the $C^{1/2}_{SUPREX}$ values obtained under similar conditions (i.e., similar LC8 concentrations and the same H/D exchange time).

Discussion

TcTex1 and LC8 have been shown to bind to diverse targets including transcription factors [TPRS-1 (12), NRF-1 (13), Swallow (32)], signaling molecules [Bim (10), nNOS (11), rhodopsin (15)], and scaffolding proteins [gephyrin (33)]. A frequent interpretation of these findings is that the LC bridges the target to the dynein motor complex and that retrograde transport of the target is the physiological consequence of this interaction (10, 15, 31). Structural investigations show that each characterized LC target binds to the same site as the dynein intermediate chain (21, 34). Sequence analysis of nearly all other reported targets (35) (J.C.W., unpublished data) suggests that they too bind to the same site. Because the LCs are homodimeric and present two identical binding surfaces, it is difficult to reconcile how the LCs can bridge identified targets to the dynein motor complex with the structural and thermodynamic measurements presented here.

Each component of the dynein motor complex is homodimeric (31, 36, 37) and thus can participate in a bivalent interaction. Bivalent or multivalent interactions are widespread in biological processes including viral and bacterial infection, cellular differentiation, immunoreactivity, and gene transcription, and they can produce significant gains in binding affinity, specificity, and functionality (reviewed in ref. 38). The generation of substantially higher affinity due to multivalency was elegantly demonstrated in studies using monovalent and trivalent vancomycin and D-Ala-D-Ala derivatives. These studies showed that dissociation

constant of monovalent vancomycin and monovalent D-Ala-D-Ala is $\approx 10^{-6}$ M, whereas the dissociation constant of the trivalent vancomycin and trivalent D-Ala-D-Ala is 10^{-17} M (25). The structure presented here shows that the LC sites can bind two IC peptide fragments simultaneously. Because the ICs are considered to be dimeric within the motor complex in physiological conditions, they should act as a bivalent ligand for the bivalent LC dimers and thus bind with higher affinity than their monovalent counterpart. The SUPREX data presented here directly confirm the enhancement of binding affinities due to multivalent interactions in this system. The bivalent IC fragment, IC_{DIMER}, binds to LC8 with higher affinity than the monovalent IC_{MONO} fragment or nNOS peptide (Fig. 3). Likewise, the preformed TcTex1, LC8, and IC_{MONO} complex is substantially more stable than either monovalent peptides.

Thus, these data suggest that, in the context of the dynein motor complex, the LCs do not bridge targets bearing the canonical LC binding sequence elements to the ICs. This is in apparent disagreement with a role for the LCs in the dynein–cargo binding interactions (Fig. 4*A*, box 1). In other words, dimeric LCs preferentially bind to dimeric targets (SI Table 5). In fact, reported LC8 and TcTex1 targets whose oligomeric properties have been characterized are dimeric (e.g., nNOS, TrkA) or predicted to be dimeric [e.g., rhodopsin, PTH receptor (39)]. Like the ICs, they too represent bivalent ligands that would preferentially bind to the bivalent LCs. In fact, it is possible that these nondynein LC targets could compete with the IC for LC binding (Fig. 4*A*, box 2). Based on our data of the monomeric nNOS peptide, which indicate that this peptide binds with higher affinity than the monomeric IC, a dimeric analog of nNOS peptide should have higher affinity. Furthermore, it is estimated that the majority of the LCs are not associated with dynein (40, 41). These estimates suggest that interaction of the LCs with the ICs represents a subset of LC targets. In other words, LCs have dynein-independent functions with multiple targets.

How such an effect might influence overall dynein structure and function is, as yet, uncertain. One function recently proposed for the LCs is to facilitate folding of the dynein IC, an intrinsically unstructured protein (42), and mediate assembly the dynein motor complex (43). Specifically, LC8 was reported to increase the α-helical content of the IC and to affect the conformation of a region of the IC C-terminal to the LC8 binding site (26). LC8 has also been reported to induce the formation of a coiled-coil in Swallow (44), further suggesting related roles in multiple proteins.

An additional attractive possibility is that the LCs regulate the function of the ICs. In fact, cytoplasmic dynein requires dynactin for many of its cellular functions (45). $p150^{Glued}$, the primary organizing subunit of this large multisubunit complex, interacts with the dynein motor complex through the ICs (6). Specifically, $p150^{Glued}$ binds residues 1–106 of the IC. This region of the IC immediately precedes the binding site for TcTex1 and LC8 (Fig. 4*B*). Splicing sites and a serine-rich region lie within the $p150^{Glued}$ binding site, suggesting that the entire region is involved in IC regulation. Phosphorylation of Ser-84 in the IC affects $p150^{Glued}$ binding (46). In this context, it is possible that the presence of the LCs regulates the conformation of N-terminal region of the IC and thus the IC interaction with dynactin. Such a role for the LCs is not without precedence. Both LC8 and TcTex1 have been shown to regulate protein function in a dynein-independent manner in other systems. For instance, LC8 binding has been shown to reverse the suppressor activity of the transcription factor TRPS1 (12), and the overexpression of TcTex1 increases voltage-dependent activity of the voltage-dependent anion-selective channel 1 (47). Finally, there is evidence that LC heterogeneity within the dynein complex can alter its function (48, 49).

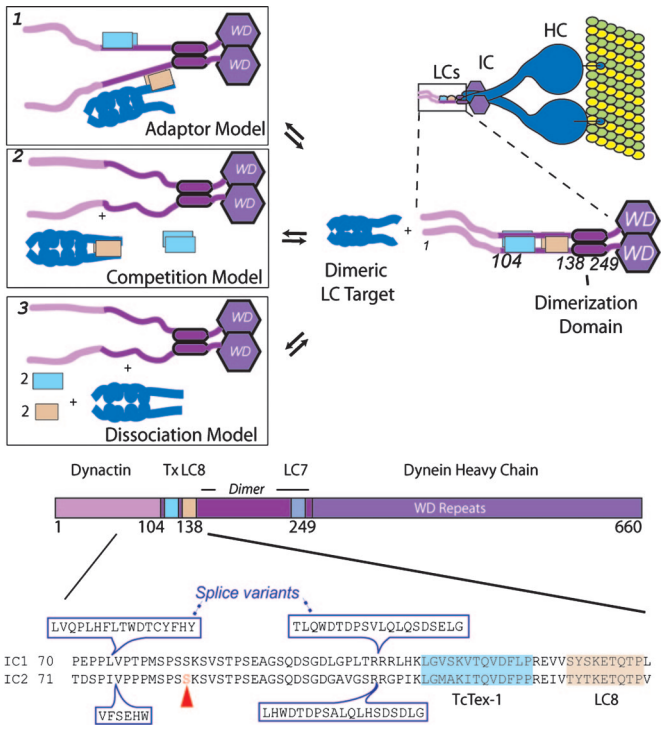

Fig. 4. Potential role of the LCs in cytoplasmic dynein. (*A*) Model based on the structure and thermodynamic characterization. A cartoon of the dynein motor complex (HC, IC, and LCs) bound to a microtubule (green/yellow) is shown in the upper right corner. The boxed region is the N-terminal half of the IC, part of which includes the IC–LC complex presented herein. The structure represents a probable state of the dynein complex ''life cycle.'' The prevalent model for the LCs in terms of cargo transport is presented in box 1. Nearly all LC8 targets encode a canonical sequence containing an invariant glutamine (see text) and bind to the same site as the IC. Because the LCs are homodimeric, one binding site can bind to the IC, and the other can bind to a putative LC cargo. However, the ICs and many of the LC targets are dimeric. Thus, they act as bivalent ligands for the bivalent LCs and thus gain affinity through energy additivity as demonstrated by our SUPREX measurements. Because many of the targets identified to bind to the LCs are dimeric, they can compete with the IC for LC binding as shown in box 2. In this model, the dimeric LC targets compete with the IC for LC binding. This would decouple the LCs from the dynein motor and negate their role in cargo transport, in disagreement with the current model. Alternatively, a posttranslation modification of the LCs or IC could lead to their dissociation. If the local concentration is less than the LC dimerization constant, the LCs could become monomeric (box 3). Monomeric LC8 cannot bind the dimeric IC (C. M. Lightcap and J.C.W., unpublished data). (*B*) Schematic of the dynein IC. The C-terminal region of the IC contains a WD domain that binds to the dynein HCs. The N-terminal region contains a strongly predicted coiled coil region, a serine rich region and variable splice sites. This N-terminal region of the IC, which is strongly predicted to be intrinsically unstructured, binds to $p150^{Glued}$ and the LCs. Phosphorylation of the IC at Ser-84 blocks the dynein–dynactin interaction.

In conclusion, our structural and thermodynamic data suggest that LC8 and TcTex1 do not directly participate in cargo transport through the canonical binding site as found in nearly all LC targets. Moreover, the weak binding of peptides that bind to the LCs despite significant buried surface area coupled with recent findings that the N terminus of the ICs are intrinsically disordered (43) suggests that the LCs may have a regulatory role.

Materials and Methods

Materials. LC8, TcTex1, and the IC peptide fragments were generated by using standard protocols (see *SI Materials and Methods*) (50). The nNOS peptide, EMKDTGIQVDR, was synthesized and purified by the protein core facility at the Kimmel Cancer Center.

Crystallization and Diffraction Studies. Crystals were obtained by using vapor diffusion in a 1:1 ratio of the protein complex (≈20 mg/ml) and the well solution (2.0–2.4 M ammonium sulfate at pH 7.0–8.0) at 4°C. SeMet TcTex1 was generated as before (22) and used to produce new crystals of the complex. The data were collected on beamline X4A (National Synchrotron Light Source). The initial partial structure was solved by molecular replacement using the TcTex1 and LC8 as models, and this information was used to find Se sites from the SAD data. SOLVE/RESOLVE (51) was used to refine the Se sites and to extract phase information for phase combination. The model was refined by using CNS (20), REFMAC (52), and O (53).

Thermodynamic Characterization. In all of the SUPREX analyses reported here, only the LC8 protein mass was monitored in the MALDI experiment (see *SI Materials and Methods*). The ΔMass values in resulting SUPREX curves correspond to the number of deuterons that had specifically exchanged into the LC8 protein. Ten replicate spectra were collected to determine the average mass change (relative to the protonated protein) at each denaturant concentration in our SUPREX experiments. These averages were used to generate LC8 SUPREX curves (i.e., plots of ΔMass versus [GdmCl]). The plots were fit to a four parameter sigmoidal equation by using SigmaPlot (Systat, San Jose, CA) to extract a $C_{\mathrm{SUPREX}}^{1/2}$ value (the denaturant concentration at the transition midpoint). The $C_{\mathrm{SUPREX}}^{1/2}$ value was plotted against exchange time according to Eq. **1** as described in ref. 27. A linear least-squares analysis was used to determine the slope and *y* intercept of the plots of $-\Delta G_{\mathrm{app}}$ versus $C_{\mathrm{SUPREX}}^{1/2}$ that were generated for the LC8 protein and for the LC8 protein complexes. These values correspond to the protein folding *m* value and folding free energy value, $\Delta G_{\mathrm{f}}^{\circ}$, respectively.

We thank members of the Williams, Fitzgerald, and Hendrickson laboratories for fruitful discussion and general support; Michael Root and Charles Scott for insightful conversation; and Lawrence Shapiro and Kevin Pfister for helpful comments on the manuscript. This work was supported in part by National Institutes of Health Grant GM34102 (to W.A.H.) and by a Career Development Award from the Leukemia and Lymphoma Society (to J.C.W.). Beamline X4A at the National Synchrotron Light Source, a U.S. Department of Energy facility, is supported by the New York Structural Biology Center.

1. Vallee RB, Wall JS, Paschal BM, Shpetner HS (1988) *Nature* 332:561–563.
2. King SM (2000) *Biochim Biophys Acta* 1496:60–75.
3. Kon T, Nishiura M, Ohkura R, Toyoshima YY, Sutoh K (2004) *Biochemistry* 43:11266–11274.
4. Gee MA, Heuser JE, Vallee RB (1997) *Nature* 390:636–639.
5. Habura A, Tikhonenko I, Chisholm RL, Koonce MP (1999) *J Biol Chem* 274:15447–15453.
6. Vaughan KT, Vallee RB (1995) *J Cell Biol* 131:1507–1516.
7. Karki S, Ligon LA, DeSantis J, Tokito M, Holzbaur EL (2002) *Mol Biol Cell* 13:1722–1734.
8. Purohit A, Tynan SH, Vallee R, Doxsey SJ (1999) *J Cell Biol* 147:481–492.
9. Pfister KK, Fisher EM, Gibbons IR, Hays TS, Holzbaur EL, McIntosh JR, Porter ME, Schroer TA, Vaughan KT, Witman GB, *et al.* (2005) *J Cell Biol* 171:411–413.
10. Puthalakath H, Huang DC, O'Reilly LA, King SM, Strasser A (1999) *Mol Cell* 3:287–296.
11. Jaffrey SR, Snyder SH (1996) *Science* 274:774–777.
12. Kaiser FJ, Tavassoli K, Van den Bemd GJ, Chang GTG, Horsthemke B, Moroy T, Ludecke HJ (2003) *Hum Mol Genet* 12:1349–1358.
13. Herzig RP, Andersson U, Scarpulla RC (2000) *J Cell Sci* 113:4263–4273.
14. Vadlamudi RK, Bagheri-Yarmand R, Yang Z, Balasenthil S, Nguyen D, Sahin AA, den Hollander P, Kumar R (2004) *Cancer Cell* 5:575–585.
15. Tai AW, Chuang JZ, Bode C, Wolfrum U, Sung CH (1999) *Cell* 97:877–887.
16. Machado RD, Rudarakanchana N, Atkinson C, Flanagan JA, Harrison R, Morrell NW, Trembath RC (2003) *Hum Mol Genet* 12:3277–3286.
17. Campbell KS, Cooper S, Dessing M, Yates S, Buder A (1998) *J Immunol* 161:1728–1737.
18. Yeh TY, Chuang JZ, Sung CH (2005) *J Cell Sci* 118:3431–3443.
19. Hendrickson WA, Horton JR, LeMaster DM (1990) *EMBO J* 9:1665–1672.
20. Brunger AT, Adams PD, Clore GM, DeLano WL, Gros P, Grosse-Kunstleve RW, Jiang JS, Kuszewski J, Nilges M, Pannu NS, *et al.* (1998) *Acta Crystallogr D* 54:905–921.
21. Liang J, Jaffrey SR, Guo W, Snyder SH, Clardy J (1999) *Nat Struct Biol* 6:735–740.
22. Williams JC, Xie H, Hendrickson WA (2005) *J Biol Chem* 280:21981–21986.
23. Aurora R, Rose GD (1998) *Protein Sci* 7:21–38.
24. Mok YK, Lo KWH, Zhang MJ (2001) *J Biol Chem* 276:14067–14074.
25. Rao J, Lahiri J, Isaacs L, Weis RM, Whitesides GM (1998) *Science* 280:708–711.
26. Barbar E, Kleinman B, Imhoff D, Li M, Hays TS, Hare M (2001) *Biochemistry* 40:1596–1605.
27. Powell KD, Fitzgerald MC (2003) *Biochemistry* 42:4962–4970.
28. Powell K, Ghaemmaghami S, Wang M, Ma L, Oas T, Fitzgerald M (2002) *J Am Chem Soc* 124:10256–10257.
29. Ma L, Fitzgerald MC (2003) *Chem Biol* 10:1205–1213.
30. Roulhac PL, Powell KD, Dhungana S, Weaver KD, Mietzner TA, Crumbliss AL, Fitzgerald MC (2004) *Biochemistry* 43:15767–15774.
31. Lo KW, Kan HM, Pfister KK (2006) *J Biol Chem* 281:9552–9559.
32. Schnorrer F, Bohmann K, Nusslein-Volhard C (2000) *Nat Cell Biol* 2:185–190.
33. Fuhrmann JC, Kins S, Rostaing P, El Far O, Kirsch J, Sheng M, Triller A, Betz H, Kneussel M (2002) *J Neurosci* 22:5393–5402.
34. Fan J, Zhang Q, Tochio H, Li M, Zhang M (2001) *J Mol Biol* 306:97–108.
35. Navarro-Lerida I, Martinez Moreno M, Roncal F, Gavilanes F, Albar JP, Rodriguez-Crespo I (2004) *Proteomics* 4:339–346.
36. Tynan SH, Gee MA, Vallee RB (2000) *J Biol Chem* 275:32769–32774.
37. Tynan SH, Purohit A, Doxsey SJ, Vallee RB (2000) *J Biol Chem* 275:32763–32768.
38. Mammen M, Choi S-K, Whitesides GM (1998) *Angew Chem Int Ed* 37:2755–2794.
39. Sugai M, Saito M, Sukegawa I, Katsushima Y, Kinouchi Y, Nakahata N, Shimosegawa T, Yanagisawa T, Sukegawa J (2003) *Biochem Biophys Res Commun* 311:24–31.
40. Tai AW, Chuang JZ, Sung CH (1998) *J Biol Chem* 273:19639–19649.
41. Chuang JZ, Yeh TY, Bollati F, Conde C, Canavosio F, Caceres A, Sung CH (2005) *Dev Cell* 9:75–86.
42. Tompa P (2002) *Trends Biochem Sci* 27:527–533.
43. Benison G, Nyarko A, Barbar E (2006) *J Mol Biol* 362:1082–1093.
44. Wang L, Hare M, Hays TS, Barbar E (2004) *Biochemistry* 43:4611–4620.
45. Schroer TA (2004) *Annu Rev Cell Dev Biol* 20:759–779.
46. Vaughan PS, Leszyk JD, Vaughan KT (2001) *J Biol Chem* 276:26171–26179.
47. Schwarzer C, Barnikol-Watanabe S, Thinnes FP, Hilschmann N (2002) *Int J Biochem Cell Biol* 34:1059–1070.
48. Kini AR, Collins CA (2001) *Cell Motil Cytoskeleton* 48:52–60.
49. Tai AW, Chuang JZ, Sung CH (2001) *J Cell Biol* 153:1499–1509.
50. Sambrook J, Fritsch EF, Maniatis T (1989) *Molecular Cloning: A Laboratory Manual* (Cold Spring Harbor Lab Press, Cold Spring Harbor, NY).
51. Terwilliger T (2004) *J Synchrotron Radiat* 11:49–52.
52. Murshudov GN, Vagin AA, Dodson EJ (1997) *Acta Crystallogr D* 53:240–255.
53. Jones TA (1978) *J Appl Crystallogr* 11:268–272.
54. Baker NA, Sept D, Joseph S, Holst MJ, McCammon JA (2001) *Proc Natl Acad Sci USA* 98:10037–10041.